Mutations in *ANO3* Cause Dominant Craniocervical Dystonia: Ion Channel Implicated in Pathogenesis

Gavin Charlesworth,[1] Vincent Plagnol,[2] Kira M. Holmström,[1] Jose Bras,[1] Una-Marie Sheerin,[1] Elisavet Preza,[1] Ignacio Rubio-Agusti,[3,4] Mina Ryten,[1,8] Susanne A. Schneider,[5] Maria Stamelou,[3] Daniah Trabzuni,[1,6,8] Andrey Y. Abramov,[1] Kailash P. Bhatia,[3,7,*] and Nicholas W. Wood[1,2,7,*]

In this study, we combined linkage analysis with whole-exome sequencing of two individuals to identify candidate causal variants in a moderately-sized UK kindred exhibiting autosomal-dominant inheritance of craniocervical dystonia. Subsequent screening of these candidate causal variants in a large number of familial and sporadic cases of cervical dystonia led to the identification of a total of six putatively pathogenic mutations in *ANO3*, a gene encoding a predicted Ca^{2+}-gated chloride channel that we show to be highly expressed in the striatum. Functional studies using Ca^{2+} imaging in case and control fibroblasts demonstrated clear abnormalities in endoplasmic-reticulum-dependent Ca^{2+} signaling. We conclude that mutations in *ANO3* are a cause of autosomal-dominant craniocervical dystonia. The locus *DYT23* has been reserved as a synonym for this gene. The implication of an ion channel in the pathogenesis of dystonia provides insights into an alternative mechanism that opens fresh avenues for further research.

Introduction

Cervical dystonia is the most common form of focal dystonia seen by neurologists.[1] Previous epidemiological studies conducted in Europe and Northern England have suggested a prevalence of 5.7–6.1 per 100,000 persons.[2,3] Although lifespan is not generally reduced, individuals affected by the condition can suffer considerable physical and psychosocial distress, which has been shown to have a significant impact on their quality of life.[4] Treatment remains symptomatic, and regular injections of botulinum toxin constitute the mainstay of current medical therapy.

Genetic factors are believed to play an important role in the pathogenesis of cervical dystonia given that around 10%–20% of affected individuals have one or more affected family members.[5,6] Despite this fact, a later age of onset and characteristically reduced penetrance have made it difficult to identify kindreds of a size sufficient to permit traditional linkage-based approaches to gene identification. So far, mutations in two genes (*TOR1A* [MIM 605204] and *THAP1* [MIM 609520]) have been conclusively shown to cause autosomal-dominant primary dystonia.[7,8] Even together, however, mutations in these genes explain only a small fraction of familial dystonia, suggesting that a number of genetic factors remain to be identified. More recently, mutations is *CIZ1* (MIM 611420) have also been suggested as a cause of adult-onset cervical dystonia,[9] although this has yet to be confirmed by others.

In this study, we combined linkage analysis with whole-exome sequencing of two individuals to identify candidate causal variants in a moderately-sized UK kindred exhibiting autosomal-dominant inheritance of primary craniocervical dystonia[10] (*TOR1A* and *THAP1* had previously been excluded). We performed Sanger sequencing of the candidate variant in a large number of dystonia samples and subsequent next-generation targeted sequencing of the whole gene to provide a comprehensive genetic screening of phenotypically similar cases.

Subjects and Methods

The Index Family

All samples were collected with the written consent of participants and formal ethical approval by the relevant research ethics committee. All living individuals from the index family were re-examined and videoed as part of this study, and the two now deceased individuals had been examined and videoed as part of a previous study.[10] The family pedigree is shown in Figure 1. All family members shown are over 25 years of age. Upon examination, all definitely affected family members exhibited tremulous cervical dystonia with a variable degree of associated upper-limb dystonic tremor. In addition, family members II-7 and III-7 had laryngeal involvement, and family member II-4 had both laryngeal involvement and blephrospasm (see Movie S1, available online). Age of onset ranged from 19–39 years, and most had onset in the last few years of their fourth decade. One family member, II-1, had additional neurological signs on examination: he exhibited mild truncal ataxia, dysarthria, and mild cognitive impairment, all dating from an episode of Wernicke-Korsakoff's encephalopathy 6 years previously. His family confirmed that he had consumed alcohol excessively for much of his life prior to that episode.

[1]Department of Molecular Neuroscience, University College London Institute of Neurology, Queen Square, London WC1N 3BG, UK; [2]University College London Genetics Institute, London WC1E 6BT, UK; [3]Sobell Department for Movement Disorders, University College London Institute of Neurology, London WC1N 3BG, UK; [4]Movement Disorders Unit, Hospital Universitario La Fe, 46009 Valencia, Spain; [5]Department of Neurology, University of Kiel, Arnold-Heller-Straße 3, 24105 Kiel, Germany; [6]King Faisal Specialist Hospital and Research Centre, Department of Genetics, PO Box 3354, Riyadh 11211, Saudi Arabia
[7]These authors contributed equally to this work
[8]On behalf of the UK Human Brain Expression Consortium
*Correspondence: n.wood@ucl.ac.uk (N.W.W.), k.bhatia@ucl.ac.uk (K.P.B.)
http://dx.doi.org/10.1016/j.ajhg.2012.10.024.

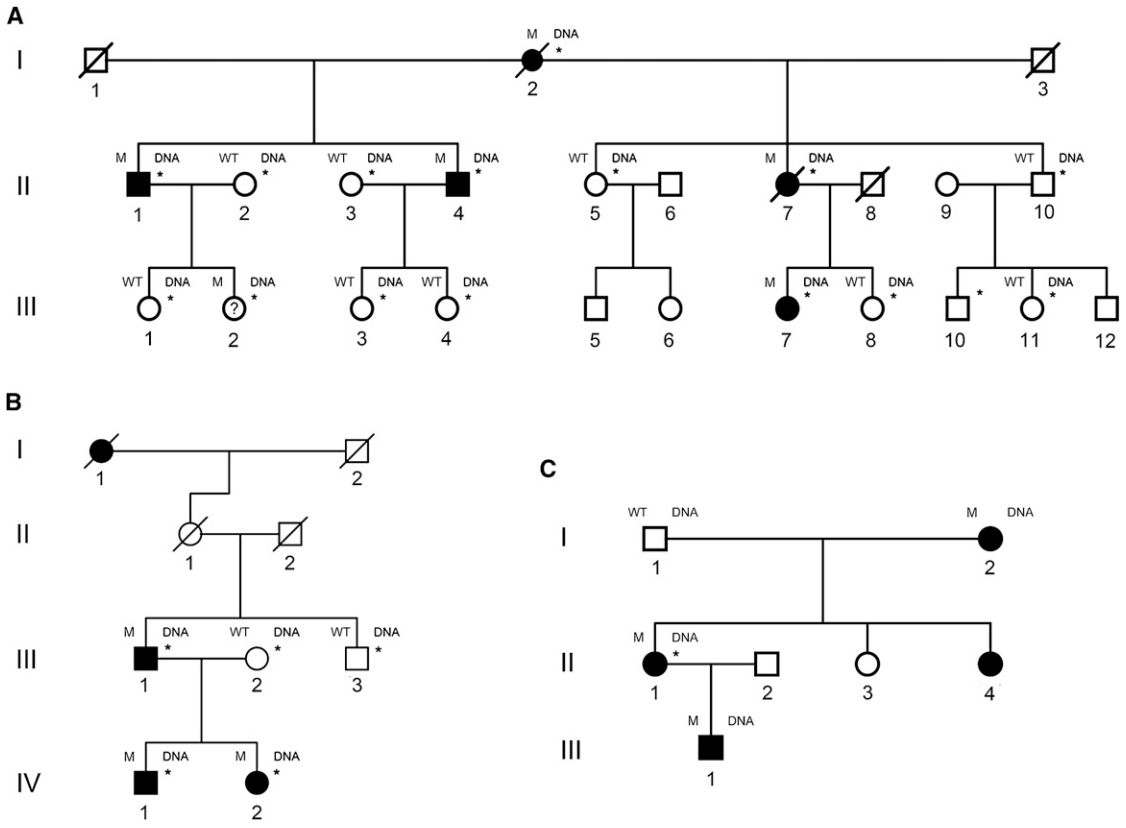

Figure 1. Family Pedigrees
(A) Pedigree showing the structure of the index family. Definitely affected family members are represented by filled symbols, and definitely unaffected family members are represented by empty symbols. The affectation status of family member III-2, represented by a circle with a question mark in the center, was uncertain. DNA was available as marked. Sequencing findings for the *ANO3* c.1480A>T (p.Arg494Trp) mutation are indicated above and to the left of each symbol. Individuals marked with an asterisk were clinically examined. The following abbreviations are used: WT, homozygous wild-type alleles; and M, heterozygous mutation carrier.
(B) Structure of the second phenotypically similar family, which carries a second, different mutation (c.1470G>C [p.Trp490Cys]) in the same exon of *ANO3*. DNA availability, examined individuals, and mutational status are marked as in (A).
(C) Structure of a third family affected by a mutation (c.2053A>G [p.Ser685Gly]) in exon 21 of *ANO3*. Individuals I-2, II-1, and III-1 exhibited onset of dystonic tremor of the head, upper limbs, and larynx in the first decade of life. Individual II-4 developed laryngeal dystonia in her late twenties. DNA availability, examined individuals, and mutational status are marked as in (A).

There was no evidence of dystonia or any other neurological signs in any definitely unaffected individual. The affectation status of one individual, represented by a circle with a question mark in the center (III-2 in Figure 1A), was uncertain. She described neck pain with a tight, pulling sensation on the left-hand side. Examination revealed a subtle left-sided torticollis, but no tremor. Given that onset for all but one member of the family affected by the disease had been in the late 30s and that she was currently 46, it was felt possible that these symptoms and examination findings might represent an early stage or a forme fruste of the condition, and so for the purpose of linkage analysis, her affectation status was set to unknown.

Genomic DNA extracted from whole blood was available for the analysis of 15 individuals. DNA from individuals III-8 and III-10 was only obtained at a late stage and was not available for linkage, but it was used for segregation analysis.

Linkage Analysis

Linkage analysis was performed by SNP genotyping with the CytoSNP-12 chip (Illumina, San Diego, CA, USA). Data from 5,652 markers, spaced at approximately equal distances across the genome, were analyzed with MERLIN (Multipoint Engine for Rapid Likelihood Inference) v.1.1.2. For the parametric analysis, LOD scores were calculated under the model of an autosomal-dominant disease with a penetrance of 80%. This produced five linkage peaks with an identical maximum LOD score of 2.01 on chromosomes 4, 5, 6, 7, and 11. The plot of LOD scores against chromosome positions is shown in Figure S1. For the five peaks with the highest LOD scores, the size of each region and number of genes contained therein are summarized in Table S1.

Whole-Exome Sequencing and Variant Calling

Three micrograms of genomic DNA from the two most distantly related, definitely affected family members (individuals II-1 and III-7) was sent to BGI (Shenzhen, China) for whole-exome capture and sequencing. This generated 57,506,202 (II-1) and 30,644,686 (III-7) unique reads per exome, translating to a total variant count of 20,935 and 17,024, respectively. According to the Consensus Coding Sequences hg19 definition of the exome, coverage was 90% and 83% for at least two reads, and the mean read depth across the exome was 46 and 45 reads, respectively.

Targeted Next-Generation Sequencing of *ANO3*

We performed targeted high-throughput sequencing of *ANO3* in 188 dystonia-affected proband samples by using the MiSeq next-generation-sequencing machine and the TruSeq Custom Amplicon kit, both supplied by Illumina. A full and detailed protocol is supplied by Illumina. In brief, custom oligonucleotides targeting all 27 *ANO3* exons (including both UTRs) were created with Illumina Design Studio. At least 25 intronic bases were included from either side of each exon. The hybridization of the oligonucleotide probes to unfragmented genomic DNA was carried out in 96-well plates and was followed by extension and ligation for the formation of DNA templates consisting of regions of interest flanked by universal primer sequences. Each plate contained 94 samples of interest, one positive control from the initial family, and one unrelated Illumina technical control well. Two hundred fifty micrograms of DNA was used as the input for the hybridization reaction. Indices and sequencing adapters supplied by Illumina were then joined by PCR reaction as per the protocol supplied with the kit. Finally, the PCR product was purified, normalized, pooled in a single tube, and sequenced on the MiSeq system. Base calling and annotation were performed by the in-built MiSeq reporter software. The average cluster density was ~700 K/mm^3, and 93% of the clusters passed quality control. No regions of the gene were poorly covered, and the average read depth across all samples was 951 reads.

Expression Profiling of *ANO3* in Brain Tissue

Expression data were obtained with Affymetrix Exon 1.0 ST Arrays and with brain and CNS tissue (originating from 137 control individuals) collected by the Medical Research Council Sudden Death Brain and Tissue Bank, Edinburgh, UK[11] and the Sun Health Research Institute, an affiliate of Sun Health Corporation, USA.[12] A full description of the samples used and the methods of RNA isolation and processing can be found in Trabzuni et al., 2011.[13] As previously described, all arrays were preprocessed with robust-multiarray-average quantile normalization with GC background correction and log2 transformation in Partek's Genomics Suite v.6.6 (Partek, St. Louis, MO, USA).[14,15] Regional differences in gene-level expression were investigated with Partek's mixed-model ANOVA, and gender and batch effects (date of hybridization and brain bank) were included as cofactors.

Ca^{2+} Imaging in Fibroblasts from Affected Individuals

After signed consent, fibroblasts were obtained from a skin biopsy from an affected individual carrying the c.1470G>C (p.Trp490Cys) mutation in *ANO3*. Age- and passage-matched controls were selected from in-house cell lines. The fibroblasts were cultured in Dulbecco's modified Eagle's medium GlutaMAX supplemented with 10% (v/v) heat-inactivated fetal bovine serum and 1% penicillin strepomycin. They were maintained at 37°C in a humidified atmosphere of 5% CO_2 and 95% air.

Cytoplasmic Ca^{2+} concentration ($[Ca^{2+}]_c$) was measured with fura-2[16] after cells were stimulated with a variety of agonists for raising $[Ca^{2+}]_c$. Cells were loaded for 30 min at room temperature with 5 μM fura-2 AM and 0.005% Pluronic in a HEPES-buffered salt solution composed of 156 mM NaCl, 3 mM KCl, 2 mM $MgSO_4$, 1.25 mM KH_2PO_4, 2 mM $CaCl_2$, 10 mM glucose, and 10 mM HEPES (pH was adjusted to 7.35 with NaOH). Ca^{2+}-free medium contained 0.5 mM EGTA. All analyzed areas were chosen at random, and three independent experiments were performed for each condition. The number of cells analyzed for each set of experiments is indicated in the Results below.

Fluorescence measurements were obtained on an epifluorescence inverted microscope equipped with a 20× fluorite objective. $[Ca^{2+}]_c$ was monitored in single cells with excitation light provided by a Xenon arc lamp, and the beam passed through a monochromator at 340 and 380 nm (Cairn Research, Kent, UK). Emitted fluorescence light was reflected through a 515 nm longpass filter to a cooled charged-coupled-device camera (Retiga, QImaging, Surrey, BC, Canada) and digitized to a 12 bit resolution. All imaging data were collected and analyzed with software from Andor (Belfast, UK). The fura-2 data were not calibrated in terms of $[Ca^{2+}]_c$ because of the uncertainty arising from the use of different calibration techniques.

ATP (100 μM) was used for stimulating $[Ca^{2+}]_c$ signals in fibroblasts via purinoceptors and for releasing calcium from the endoplasmic reticulum (ER) via IP3 receptors. Fifty millimolars of KCl was used for inducing depolarization of the plasma membrane and for opening voltage-gated calcium channels. Thapsigargin (1 μM) in Ca^{2+}-free medium (plus 0.5 mM EGTA) was used for inducing the release of calcium from the ER to the cytosol and thus for estimating the size of the reticular Ca^{2+} pool.

Results

Variant analysis of exome-sequencing data was based on the assumption that the mutation causing this uncommon, heritable form of the disease in this family would not be present in the general population at an appreciable frequency. In order to maximize the chances of isolating the causal variant and to minimize the chances of error in assignment, we employed two different strategies to select candidate causal variants. The first strategy involved selecting only those variants that were present in the exome data of both affected family members for analysis. Homozygous variants, synonymous variants, and variants recorded in dbSNP135 were initially removed. We then filtered out any variant present at a global minor allele frequency (MAF) $\geq$ 1% in a range of publically available databases of sequence variation (1000 Genomes, Complete Genomic 69 Database, and the National Heart, Lung, and Blood Institute [NHLBI] Exome Sequencing Project database), as well as those found in two or more of our own in-house exomes from individuals (n = 200) with unrelated diseases. Finally, variants within the regions under the linkage peaks with the highest LOD scores (on chromosomes 4, 5, 6, 7, and 11; see Table S1 for definition of regions) were validated by Sanger sequencing in the forward and reverse directions with the use of BigDye Terminator v.3.1 chemistry and the Applied Biosystems 3130XL Genetic Analyzer (Life Technologies, Carlsbad, CA, USA) and were checked for segregation. This strategy revealed three potentially pathogenic variants. The first, a heterozygous frameshift deletion (c.166-167del [p.Trp56fs]) in exon 2 of *TBC1D7* (MIM 612655; RefSeq accession number NM_016495.4) on chromosome 4, failed to fully segregate, given that individual II-5, who is unaffected at age 61, and individual III-8,

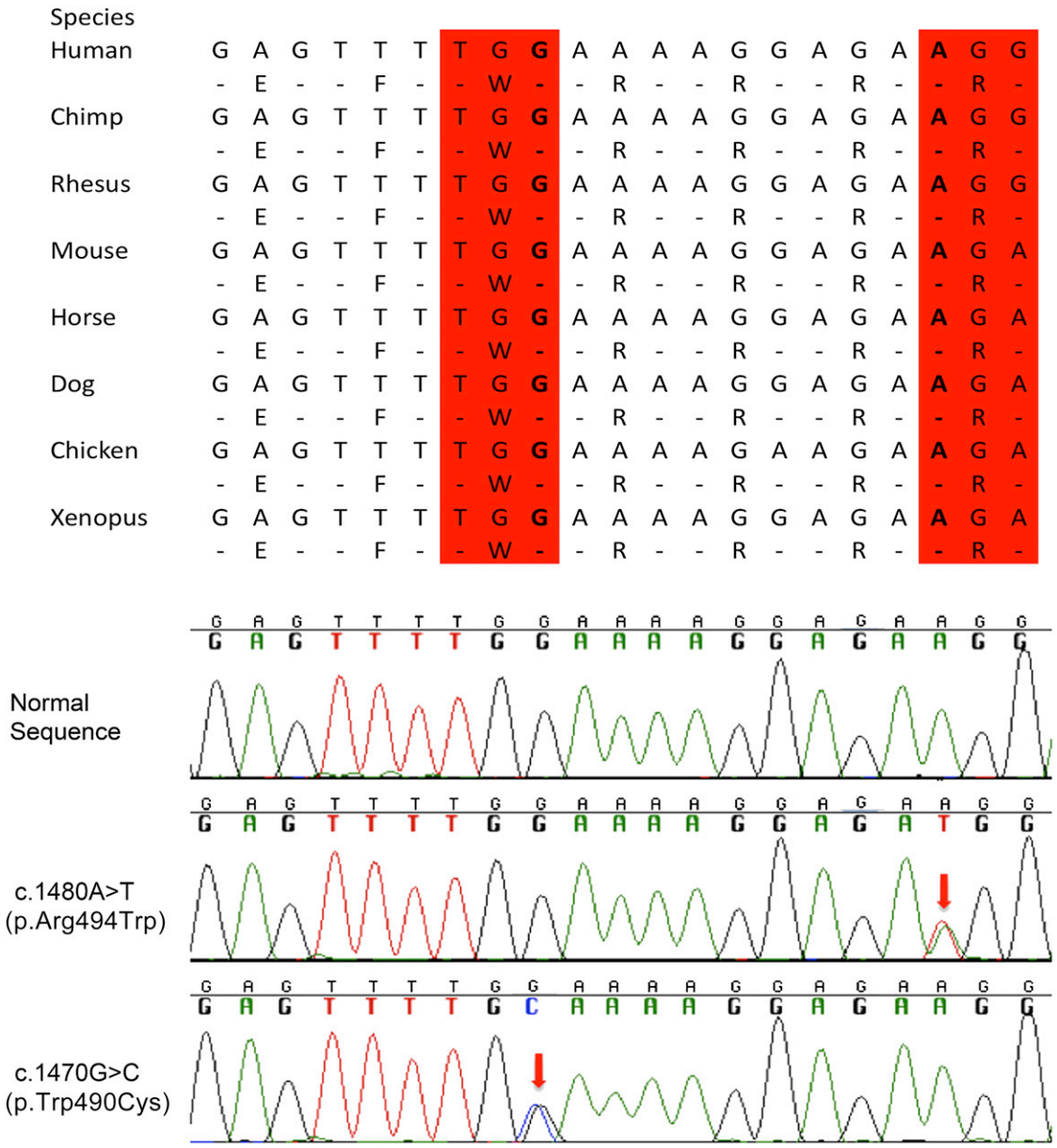

Figure 2. Mutations in Exon 15 of *ANO3*
Diagram showing complete conservation of protein sequence and almost complete conservation of amino acid sequence across species in the region of exon 15 of *ANO3*, in which two disease-segregating mutations (c.1480A>T [p.Arg494Trp] and c.1470G>C [p.Trp490Cys]) were found (the affected bases and codons are shown in boldface and red, respectively). At the bottom, aligned electropherograms show normal and mutated sequences.

who is unaffected at age 32, exhibit the deletion. The second was a heterozygous missense variant (c.77G>A [p.Arg26His]) in exon 2 of *PPM1K* (MIM 611065; RefSeq NM_152542.3) on chromosome 4. It was not predicted to be damaging by MutationTaster, SIFT, or PolyPhen-2 and was found at a low frequency in African American samples (2 out of 4,404) in the NHLBI exome data. Also, it did not segregate, given that definitely unaffected individual III-1, who is 42 years of age, and III-8, who is 32 years of age, carry the variant. The third, a missense mutation (c.1480A>T [p.Arg494Trp]) in exon 15 of *ANO3* (MIM 610110; RefSeq NM_031418.2) on chromosome 11, segregated perfectly with the disease status in definitely affected and unaffected individuals. In addition, the individual of uncertain affectation status was also seen to carry the variant. The mutation occurred at a base that was highly conserved between species (see Figure 2), resulting in a change from arginine to tryptophan at position 494 of the protein, and was predicted to be damaging by MutationTaster, SIFT, and PolyPhen-2.

In order to compensate for any unequal coverage between the two exomes, we employed a second strategy, in which all variants from the exome with the best coverage were first filtered as above, to produce a list of

every nonsynonymous single-nucleotide variant or frameshift and nonframeshift indel not recorded in dbSNP135 or in public databases of sequence variation at a global MAF $\geq$ 1%. We then discarded any variants that were not in areas covered by the linkage peaks with the highest LOD scores (see Table S1). For each remaining variant in turn, we then visually inspected the data for the other exome to ensure that it had been covered. If it had not been covered adequately (as in the case of two variants), the exon of the gene containing the variant was Sanger sequenced and, if present, checked for segregation in the rest of the family. The results are detailed in Table S2, but in summary, this strategy did not identify any new candidate variants that segregated with the disease.

Screening of *ANO3* Exon 15 in Additional Cases Revealed a Second Segregating Mutation

We next took our best candidate variant in exon 15 of *ANO3* and Sanger sequenced the exon in a selection of phenotypically similar cases. As an additional check, in the same selection of cases, we also sequenced the exons containing the variant of the two genes (*TBC1D7* and *TMEM232*) that had failed to segregate solely because of the presence of the variant in a single unaffected individual. We did this to account for the possibility of a reduced penetrance, which appears to be common in dystonia. DNA samples for sequencing were obtained from an in-house library of previously donated samples from individuals who had given research consent. Samples were selected on the basis that the accompanying clinical description suggested cervical dystonia and/or dystonic upper-limb tremor. Both familial (n = 137) and sporadic (n = 247) cases were selected for inclusion. Samples that were known to have previously tested positive for *TOR1A* or *THAP1* were excluded. We also included a small number of samples from individuals for whom the primary clinical impression had been of familial essential tremor or myoclonus dystonia (provided they tested negative for mutations in *SGCE* [MIM 604149]) because it was felt that these clinical phenotypes might easily be confused with upper-limb dystonic tremor or jerky cervical dystonia, respectively.[17] A total of 384 samples were screened.

Analysis of the sequence traces for these 384 individuals revealed no potentially pathogenic variants in exon 2 of *TBC1D7* or exon 10 of *TMEM232*. In exon 15 of *ANO3*, however, we found a second heterozygous missense mutation (c.1470G>C [p.Trp490Cys]) in the same highly conserved region in which the mutation in the index family was located (see Figure 2); this second mutation was also predicted to be damaging by SIFT, PolyPhen-2, and MutationTaster. It was not present in the data from the NHLBI Exome Sequencing Project (4,090 $\pm$ 627 samples of European ancestry at a read depth of 80 $\pm$ 40), 1000 Genomes Project, or our own in-house exomes (n = 200). The phenotype of the individual (IV-2 in Figure 1B) in whom the mutation was found was almost identical to that of the initial index family; she had tremulous cervical dystonia with laryngeal involvement and a dystonic tremor of the upper limbs (see Movie S2). Onset was in the early teens, and the fact that her brother and father were also affected suggests autosomal-dominant inheritance. DNA samples were obtained from all available members of the family, which confirmed that both the father (III-1) and brother (IV-1) carried the variant but that the father's unaffected brother (III-3) did not. Interestingly, her paternal great grandmother (I-1), but not her paternal grandmother (II-1), was reported to have been affected by head tremor. Although both individuals are now deceased and could not be examined, this suggests the possibility that penetrance might not be complete.

High-Throughput Sequencing of the Whole *ANO3* Reveals Four Additional Variants

On the basis of the finding of a second mutation, we performed targeted high-throughput sequencing of *ANO3* in 188 samples by using the MiSeq next-generation-sequencing machine and the TruSeq Custom Amplicon kit, both supplied by Illumina. A total of 110 familial and 78 sporadic samples, selected as above, were screened.

We identified four putative pathogenic variants: three missense variants in exons 2, 21, and 25 and a variant in the 5′ UTR (summarized in Table 1 and shown on Figure S2). None of these variants were seen in the publically available data from the NHLBI Exome Sequencing Project, 1000 Genomes Project, or our own in-house exomes. In silico predictions of their pathogenicity by MutationTaster, SIFT, and PolyPhen-2 were, however, contradictory (see Table 1 for individual results). Clinically, two of the four individuals had cervical dystonia, and three of the four individuals had upper-limb tremor. The individual carrying a mutation (c.2053A>G [p.Ser685Gly]) in exon 21 of *ANO3* had a clear autosomal-dominant history of cervical, laryngeal, and upper-limb tremulous dystonia (see Figure 1C). She (II-1), her mother (I-2), and her son (III-1) had all developed symptoms in their first decade of life. We were able to obtain DNA samples from her mother and son; both individuals were heterozygous for the c.2053A>G mutation. Her father was homozygous for the normal allele. She also reported one unaffected sister and one sister who developed laryngeal dystonia in her late twenties. Unfortunately, these individuals currently reside outside of the UK, and it was not possible to obtain DNA from them. We were also unable to obtain DNA for segregation for the variants in the UTR, exon 2, or exon 25 either because of social circumstances or because the affected relatives were deceased or did not wish to take part in the study.

ANO3 Is Most Highly Expressed in the Striatum

We then investigated the expression of *ANO3* in brain and CNS tissues by using in-house data from the UK Brain Expression Consortium. The regional distribution of *ANO3* mRNA expression at the gene level is shown in Figure 3A. This demonstrated significant regional

Table 1. Additional *ANO3* Variants Identified by High-Throughput Sequencing

Location within Transcript (RefSeq NM_031418.2)	cDNA Mutation	Protein Alteration	MutationTaster Prediction	SIFT Prediction	PolyPhen-2 Prediction	Clinical Phenotype of Case
Exon 2	c.161C>T	p.Thr54Ile	polymorphism	tolerated	benign	diagnosed as "familial essential tremor;" individual not contactable
Exon 21	c.2053A>G	p.Ser685Gly	disease causing	tolerated	benign	early-onset (first decade of life) autosomal-dominant cervical dystonia, dystonic tremor of the upper limbs, and laryngeal dystonia; the mother, one sister, and son were also affected; the sister was affected later and by laryngeal dystonia only
Exon 25	c.2586G>T	p.Lys862Asn	disease causing	tolerated	benign	cervical dystonia and oromandibular dystonia; deceased father was also affected
5′ UTR	c.-190C>T	-	disease causing	no prediction	no prediction	cervical dystonia and upper-limb tremor since late teens; myoclonic jerks; diagnosed as myoclonus dystonia, but *SGCE* testing was negative; no family history on maternal side, but father not seen since birth

Variants identified by high-throughput targeted sequencing of all 27 *ANO3* exons and both UTRs, as well as in silico predictions of pathogenicity and brief clinical descriptions of the cases. None of these variants were in publically available data from the NHLBI Exome Sequencing Project, 1000 Genomes Project, or our own in-house exomes.

differences in *ANO3* mRNA expression: there was an 5.3-fold difference (p value $< 1.0 \times 10^{-45}$) between the putamen, the highest *ANO3*-expressing region, and the frontal cortex, the region with the second highest expression, and there was a 70-fold difference in expression between the putamen and the cerebellum, the region with the lowest expression (p value $< 1.0 \times 10^{-45}$). These findings are consistent with those of Kang et al., 2011[18] and Johnson et al., 2009,[19] which demonstrate increasing expression of *ANO3* mRNA during the course of human brain development—particularly within the striatum but also the neocortex, hippocampus, and amygdala (Figure 3B)—from early midfetal development (between 13 and 16 post-conception weeks of age) to adolescence (between 12 and 20 years of age).

Fibroblasts from Affected Individuals Demonstrate ER-Related Calcium-Signaling Abnormalities

ANO3 belongs to a family of genes that are thought to encode ion channels, more specifically Ca^{2+}-activated Cl^- channels.[20] Therefore, in order to investigate the influence of the *ANO3* mutations on calcium homeostasis, we measured $[Ca^{2+}]_c$ by using fura-2 after treating cells with ATP, potassium chloride (KCl), and thapsigargin. In the text below, "n" indicates the number of cells analyzed for each set of experiments, which were carried out in triplicate.

Initially, we used ATP (100 μM) to stimulate $[Ca^{2+}]_c$ signals in fibroblasts via purinoceptors and to release calcium from the ER via IP3 receptors. We then applied 50 mM KCl to induce depolarization of the plasma membrane and open voltage-gated calcium channels. We found that fibroblasts from the affected individual carrying the c.1470G>C (p.Trp490Cys) mutation showed significantly less ATP-induced calcium signal (Figures 4A and 4B; $n = 41$; $p < 0.05$) than did control cells. Importantly, the application of 50 mM KCl induced a similar rise in $[Ca^{2+}]_c$ in both control fibroblasts (ctrl 1 [$n = 56$] and ctrl 2 [$n = 33$]) and in fibroblasts with the c.1470G>C (p.Trp490Cys) mutation in *ANO3* (Figure 4B). Thus, in response to ATP, the *ANO3* mutation resulted in a reduced calcium signal, which can most likely be explained by a smaller calcium pool within the ER. The similar responses in control and mutation-carrying cells seen upon depolarization of the plasma membrane suggest that the mutation does not modulate voltage-gated calcium channels or active Ca^{2+} transport (the mechanism of calcium removal from the cytosol).

To confirm these findings, we performed further experiments by using thapsigargin (1 μM) in Ca^{2+}-free medium (plus 0.5 mM EGTA). The addition of thapsigargin, which is an inhibitor of the sarcoplasmic ER calcium ATPase, induces a release of calcium from the ER to the cytosol and can be used for estimating the reticular Ca^{2+}-pool. Adding Ca^{2+} at the end of the experiment stimulated elevation of $[Ca^{2+}]_c$ in fibroblasts (Figure 4C) as a result of the opening of store-operated calcium channels. We found that the calcium signal in response to thapsigargin in fibroblasts carrying the c.1470G>C (p.Trp490Cys) mutation was significantly smaller ($n = 26$; $p < 0.001$; Figures 4C and 4D) than that in ctrl 1 ($n = 19$) and ctrl 2 ($n = 22$). This strongly suggests that the thapsigargin-sensitive Ca^{2+} pool in the ER of mutation-carrying fibroblasts is significantly smaller than that in control cells. Stimulation of the store-operated Ca^{2+} channels induced similar elevation of $[Ca^{2+}]_c$ in control and mutated fibroblasts (Figures 4C and 4D).

Discussion

In a moderately-sized UK kindred affected by apparently autosomal-dominant craniocervical dystonia and dystonic

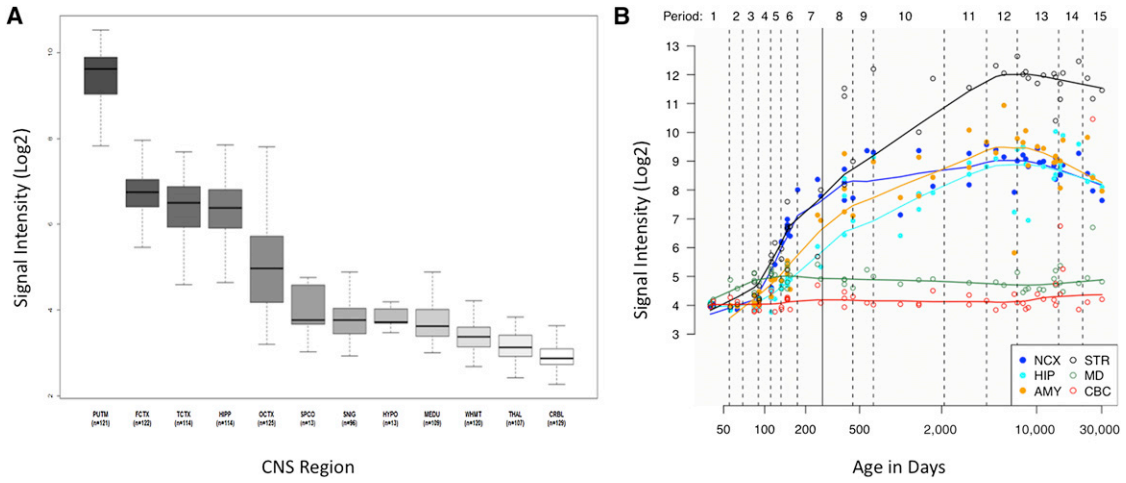

Figure 3. Graphical Summary of Expression Data

(A) Box plot of *ANO3* mRNA expression levels in 12 CNS regions. The expression levels are based on exon array experiments and are plotted on a log2 scale (*y* axis). This plot shows significant variation in *ANO3* transcript expression across the 12 CNS regions analyzed: putamen (PUTM, n = 121), frontal cortex (FCTX, n = 122), temporal cortex (TCTX, n = 114), hippocampus (HIPP, n = 114), cervical spinal cord (SPCO, n = 13), substantia nigra (SNIG, n = 96), hypothalamus (HYPO, n = 13), medulla (specifically inferior olivary nucleus, MEDU, n = 109), intralobular white matter (WHMT, n = 120), thalamus (THAL, n = 107), and cerebellar cortex (CRBL, n = 129). *ANO3* mRNA expression is significantly higher in the putamen than in all other brain regions. Whiskers extend from the box to 1.5× the interquartile range.

(B) Graph to show *ANO3* mRNA expression levels in six brain regions during the course of human brain development. The expression levels are based on exon array experiments and are plotted on a log2 scale.[18,19] The brain regions analyzed are the striatum (STR), amygdala (AMY), neocortex (NCX), hippocampus (HIP), mediodorsal nucleus of the thalamus (MD), and cerebellar cortex (CBC). This plot shows increasing expression of *ANO3* mRNA during human brain development, particularly in the striatum, from the early midfetal period to adolescence.

tremor, we performed linkage analysis and exome sequencing to identify candidate causal variants. On the basis of this approach, our top candidate was a missense variant (c.1480A>T [p.Arg494Trp]) in exon 15 of *ANO3*. Further sequencing of this *ANO3* exon revealed a second small family affected by an almost identical phenotype; ten bases upstream of c.1480A>T, a second missense variant (c.1470G>C [p.Trp490Cys]) segregating with the disease was identified in those family members available for testing. Neither variant in exon 15 was seen in the publically available data from the NHLBI Exome Sequencing Project, 1000 Genomes Project, or our own in-house exomes, and both were predicted to be deleterious by SIFT, PolyPhen-2, and MutationTaster. Subsequent targeted high-throughput sequencing of the entire gene in 188 individuals revealed three further coding variants and one variant in the 5′ UTR in individuals with tremulous cervical dystonia and/or upper-limb tremor. Although these variants were not recorded in the above databases, predictions of their pathogenicity were contradictory, and further functional work or mutational screening will be required for firmly establishing their link to dystonia. However, at least one (c.2053A>G [p.Ser685Gly]) of these additional variants appeared to segregate with disease in the family members available for testing.

ANO3 encodes a protein called anoctamin 3, about which little is yet known. It belongs to a family of genes (*ANO1–ANO10*) that appear to be closely related in sequence and topology but that have distinct expression patterns.[21,22] Members of the family are found throughout eukaryotes, including mammals, flies, worms, plants, protozoa, and yeast, but are best represented in higher vertebrates that possess the most members.[23] Moreover, many of these genes have been linked to disease, suggesting that they play an important role within their specific tissue types. For instance, mutations in *ANO1* (MIM 610108) have been linked to cancer,[24] mutations in *ANO5* (MIM 608662) have been linked to several forms of muscular dystrophy,[25,26] mutations in *ANO10* (MIM 613726) have been linked to autosomal-recessive spinocerebellar ataxia,[27] and mutations in *ANO6* (MIM 608663) have been linked to Scott syndrome, a rare bleeding disorder.[28]

ANO1 and *ANO2* (MIM 610109), the best studied members of the family, encode proteins that function as Ca^{2+}-activated chloride channels (CaCCs).[29] It remains an open question as to whether anoctamin 3 functions in the same manner. Hydropathy analysis suggests a similar topology—eight hydrophobic helices have been found to be likely transmembrane domains and cytosolic N and C termini (see Figure S2)—but more recent work has suggested that anoctamin 3 might in fact be targeted to the ER rather than to the cell surface (like anoctamins 1 and 2).[20] CaCCs are, nonetheless, known to have a role in the modulation of neuronal excitability,[30,31] and, in view of our data showing very high expression of *ANO3* in the striatum, it is possible that mutations in this gene lead to abnormal striatal-neuron excitability, which manifests

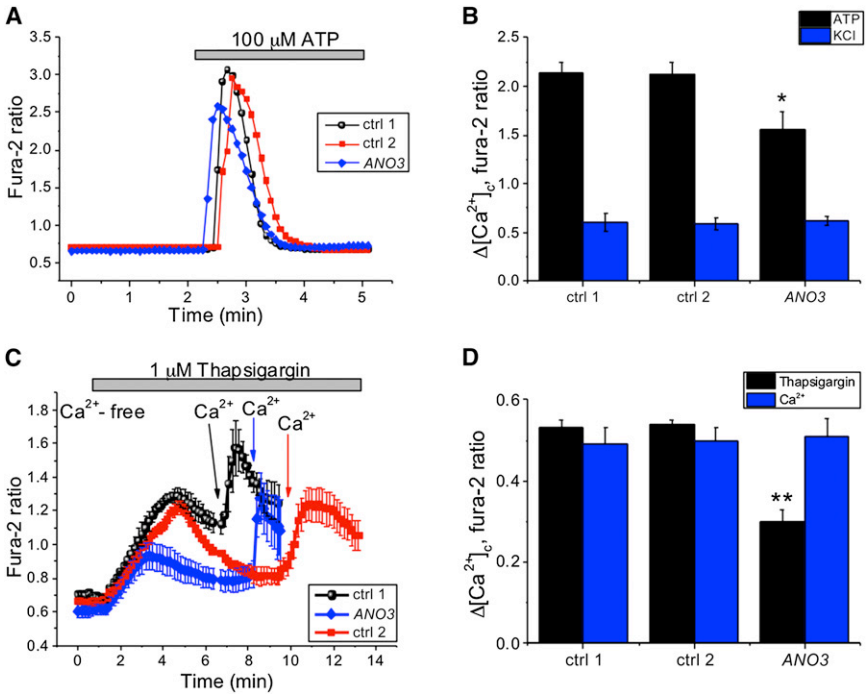

Figure 4. Graphical Summary of Fibroblast Functional Studies

(A) Typical trace of $[Ca^{2+}]_c$, as measured by fura-2, in control (ctrl 1 and ctrl 2) and mutation-bearing (*ANO3* c.1470G>C [p.Trp490Cys]) fibroblasts in response to the application of 100 μM ATP.

(B) A histogram shows a significantly decreased change in $[Ca^{2+}]_c$ in response to 100 μM ATP (black bars) in mutation-bearing fibroblasts and no change in $[Ca^{2+}]_c$ in response to 50 mM KCl (blue bars). Error bars represent the SEM, and the asterisk indicates $p < 0.05$.

(C) Mean trace of $[Ca^{2+}]_c$ in response to thapsigargin (1 μM) and subsequent Ca^{2+} (2 mM) challenge (arrows). Error bars represent the SEM.

(D) Histograms demonstrate a significant difference in ER calcium pool in *ANO3*-mutant cells compared to controls in response to thapsigargin (black bars) but no changes in the activation of store-operated calcium channels in response to the subsequent calcium challenge (blue bars). Error bars represent the SEM, and the double asterisks indicate $p < 0.001$.

itself clinically in unwanted dystonic movements. In this regard, it is interesting to note that the two mutations that we found in exon 15 lead to amino acid changes within a predicted cytosolic loop that some have suggested might function as the Ca^{2+} sensor.[21] Indeed, mutations in the homologous loop of *AN03*'s sister gene, *ANO2*, have recently been shown to alter the voltage dependence of channel activation.[32] Our own data from fibroblasts carrying a mutation in exon 15 of *ANO3* confirm abnormalities in Ca^{2+} signaling. The lack of a difference in Ca^{2+} response to KCl, which would be expected to open ion channels in the plasmalemma in the context of a significantly reduced response to two agents known to cause calcium release from the ER (ATP and, more specifically, thapsigargin), suggests a potential defect in ER-related Ca^{2+} handling in these mutation-bearing fibroblasts.

A third mutation (c.2053A>G [p.Ser685Gly]) was found in the loop between the fifth and sixth transmembrane domains of the protein (see Figure S2). In anoctamin 1, it is thought that this loop might form a critical component of the channel pore,[33] although there is debate about whether this loop is extracellular, reentrant, or cytosolic.[34] If anoctamin 3 were also proven to function as an ion channel, this work might suggest a possible mechanism by which an amino acid substitution in this loop could confer pathogenicity.

Although further functional work will be required for establishing the mechanism by which mutations in *ANO3* might lead to dystonia, the implication of a transmembrane ion channel in the pathogenesis of this condition represents a completely fresh avenue of inquiry for future research in this field and, importantly, raises the possibility that pharmaceutical agents targeted at compensating for aberrant channel function could potentially be beneficial in the treatment of a subset of dystonia-affected individuals. For instance, CaCCs can be blocked in vitro by niflumic acid, by tamoxifen, and, to a lesser extent and in a less specific manner, by fluoxetine.[31] Finally, it will be important to carry out further genetic screening of phenotypically similar cases in this and other populations in order to establish the prevalence of mutations in this gene as a cause of autosomal-dominant cervical dystonia, dystonic head tremor, and/or upper-limb dystonic tremor.

Supplemental Data

Supplemental Data include two figures, two tables, and two movies and can be found with this article online at http://www.cell.com/AJHG.

Acknowledgments

We would like to extend our thanks to the individuals whose participation made this research possible. This work was supported financially by a strategic award (WT089698/Z/09/Z) from the Medical Research Council and Wellcome Trust. The funders had no role in the study design, data collection and analysis, decision to publish, or preparation of the manuscript. This work was undertaken at University College London Hospitals and University College London (UCL), which receive support from the funding streams of the Department of Health's National Institute for Health Research Biomedical Research Centres. Expression data were provided by the UK Human Brain Expression Consortium (UKBEC), which comprises John A. Hardy, Mina Ryten, Daniah Trabzuni, Michael Weale, Adaikalavan Ramasamy, Colin Smith, and Robert Walker. UKBEC members are affiliated with the UCL Institute of Neurology (J.A.H., M.R., and D.T.), King's College London (M.W. and A.R.), and the University of Edinburgh (C.S.

and R.W). Kailash P. Bhatia received advisor, honorarial, and financial support to attend and speak at meetings from GlaxoSmithKline, Boehringer-Ingelheim, Ipsen, Merz, and Orion Pharma. He holds research grants from the Dystonia Society UK and the Halley Stewart Trust.

Received: August 16, 2012
Revised: September 21, 2012
Accepted: October 25, 2012
Published online: November 29, 2012

Web Resources

The URLs for data presented herein are as follows:

1000 Genomes Project, http://www.1000genomes.org/
Complete Genomics, http://www.completegenomics.com/public-data/69-Genomes/
dbSNP, http://www.ncbi.nlm.nih.gov/projects/SNP/
MERLIN, http://www.sph.umich.edu/csg/abecasis/merlin/index.html
MutationTaster, http://www.mutationtaster.org/
NHLBI Grand Opportunity Exome Sequencing Project, https://esp.gs.washington.edu/drupal/
Online Mendelian Inheritance in Man (OMIM), http://www.omim.org
PolyPhen-2, http://genetics.bwh.harvard.edu/pph2/
SIFT, http://sift.jcvi.org/

References

1. Velickovic, M., Benabou, R., and Brin, M.F. (2001). Cervical dystonia pathophysiology and treatment options. Drugs *61*, 1921–1943.
2. Epidemiological Study of Dystonia in Europe (ESDE) Collaborative Group. (2000). A prevalence study of primary dystonia in eight European countries. J. Neurol. *247*, 787–792.
3. Duffey, P.O., Butler, A.G., Hawthorne, M.R., and Barnes, M.P. (1998). The epidemiology of the primary dystonias in the north of England. Adv. Neurol. *78*, 121–125.
4. Skogseid, I.M., Malt, U.F., Røislien, J., and Kerty, E. (2007). Determinants and status of quality of life after long-term botulinum toxin therapy for cervical dystonia. Eur. J. Neurol. *14*, 1129–1137.
5. Chan, J., Brin, M.F., and Fahn, S. (1991). Idiopathic cervical dystonia: Clinical characteristics. Mov. Disord. *6*, 119–126.
6. Defazio, G., Aniello, M.S., Masi, G., Lucchese, V., De Candia, D., and Martino, D. (2003). Frequency of familial aggregation in primary adult-onset cranial cervical dystonia. Neurol. Sci. *24*, 168–169.
7. Ozelius, L.J., Hewett, J.W., Page, C.E., Bressman, S.B., Kramer, P.L., Shalish, C., de Leon, D., Brin, M.F., Raymond, D., Corey, D.P., et al. (1997). The early-onset torsion dystonia gene (DYT1) encodes an ATP-binding protein. Nat. Genet. *17*, 40–48.
8. Fuchs, T., Gavarini, S., Saunders-Pullman, R., Raymond, D., Ehrlich, M.E., Bressman, S.B., and Ozelius, L.J. (2009). Mutations in the THAP1 gene are responsible for DYT6 primary torsion dystonia. Nat. Genet. *41*, 286–288.
9. Xiao, J., Uitti, R.J., Zhao, Y., Vemula, S.R., Perlmutter, J.S., Wszolek, Z.K., Maraganore, D.M., Auburger, G., Leube, B., Lehnhoff, K., and LeDoux, M.S. (2012). Mutations in CIZ1 cause adult onset primary cervical dystonia. Ann. Neurol. *71*, 458–469.
10. Münchau, A., Valente, E.M., Davis, M.B., Stinton, V., Wood, N.W., Quinn, N.P., and Bhatia, K.P. (2000). A Yorkshire family with adult-onset cranio-cervical primary torsion dystonia. Mov. Disord. *15*, 954–959.
11. Millar, T., Walker, R., Arango, J.C., Ironside, J.W., Harrison, D.J., MacIntyre, D.J., Blackwood, D., Smith, C., and Bell, J.E. (2007). Tissue and organ donation for research in forensic pathology: The MRC Sudden Death Brain and Tissue Bank. J. Pathol. *213*, 369–375.
12. Beach, T.G., Sue, L.I., Walker, D.G., Roher, A.E., Lue, L., Vedders, L., Connor, D.J., Sabbagh, M.N., and Rogers, J. (2008). The Sun Health Research Institute Brain Donation Program: description and experience, 1987-2007. Cell Tissue Bank. *9*, 229–245.
13. Trabzuni, D., Ryten, M., Walker, R., Smith, C., Imran, S., Ramasamy, A., Weale, M.E., and Hardy, J. (2011). Quality control parameters on a large dataset of regionally dissected human control brains for whole genome expression studies. J. Neurochem. *119*, 275–282.
14. Irizarry, R.A., Bolstad, B.M., Collin, F., Cope, L.M., Hobbs, B., and Speed, T.P. (2003). Summaries of Affymetrix GeneChip probe level data. Nucleic Acids Res. *31*, e15.
15. Trabzuni, D., Wray, S., Vandrovcova, J., Ramasamy, A., Walker, R., Smith, C., Luk, C., Gibbs, J.R., Dillman, A., Hernandez, D.G., et al. (2012). MAPT expression and splicing is differentially regulated by brain region: Relation to genotype and implication for tauopathies. Hum. Mol. Genet. *21*, 4094–4103.
16. Vaarmann, A., Gandhi, S., Gourine, A.V., and Abramov, A.Y. (2010). Novel pathway for an old neurotransmitter: Dopamine-induced neuronal calcium signalling via receptor-independent mechanisms. Cell Calcium *48*, 176–182.
17. Quinn, N.P., Schneider, S.A., Schwingenschuh, P., and Bhatia, K.P. (2011). Tremor—Some controversial aspects. Mov. Disord. *26*, 18–23.
18. Kang, H.J., Kawasawa, Y.I., Cheng, F., Zhu, Y., Xu, X., Li, M., Sousa, A.M., Pletikos, M., Meyer, K.A., Sedmak, G., et al. (2011). Spatio-temporal transcriptome of the human brain. Nature *478*, 483–489.
19. Johnson, M.B., Kawasawa, Y.I., Mason, C.E., Krsnik, Ž., Coppola, G., Bogdanović, D., Geschwind, D.H., Mane, S.M., State, M.W., and Šestan, N. (2009). Functional and evolutionary insights into human brain development through global transcriptome analysis. Neuron *62*, 494–509.
20. Duran, C., Qu, Z., Osunkoya, A.O., Cui, Y., and Hartzell, H.C. (2012). ANOs 3-7 in the anoctamin/Tmem16 Cl- channel family are intracellular proteins. Am. J. Physiol. Cell Physiol. *302*, C482–C493.
21. Milenkovic, V.M., Brockmann, M., Stöhr, H., Weber, B.H., and Strauss, O. (2010). Evolution and functional divergence of the anoctamin family of membrane proteins. BMC Evol. Biol. *10*, 319.
22. Gritli-Linde, A., Vaziri Sani, F., Rock, J.R., Hallberg, K., Iribarne, D., Harfe, B.D., and Linde, A. (2009). Expression patterns of the Tmem16 gene family during cephalic development in the mouse. Gene Expr. Patterns *9*, 178–191.
23. Duran, C., and Hartzell, H.C. (2011). Physiological roles and diseases of Tmem16/Anoctamin proteins: Are they all chloride channels? Acta Pharmacol. Sin. *32*, 685–692.
24. Duvvuri, U., Shiwarski, D.J., Xiao, D., Bertrand, C., Huang, X., Edinger, R.S., Rock, J.R., Harfe, B.D., Henson, B.J., Kunzelmann,

K., et al. (2012). TMEM16A induces MAPK and contributes directly to tumorigenesis and cancer progression. Cancer Res. *72*, 3270–3281.

25. Bolduc, V., Marlow, G., Boycott, K.M., Saleki, K., Inoue, H., Kroon, J., Itakura, M., Robitaille, Y., Parent, L., Baas, F., et al. (2010). Recessive mutations in the putative calcium-activated chloride channel Anoctamin 5 cause proximal LGMD2L and distal MMD3 muscular dystrophies. Am. J. Hum. Genet. *86*, 213–221.
26. Penttilä, S., Palmio, J., Suominen, T., Raheem, O., Evilä, A., Muelas Gomez, N., Tasca, G., Waddell, L.B., Clarke, N.F., Barboi, A., et al. (2012). Eight new mutations and the expanding phenotype variability in muscular dystrophy caused by ANO5. Neurology *78*, 897–903.
27. Vermeer, S., Hoischen, A., Meijer, R.P., Gilissen, C., Neveling, K., Wieskamp, N., de Brouwer, A., Koenig, M., Anheim, M., Assoum, M., et al. (2010). Targeted next-generation sequencing of a 12.5 Mb homozygous region reveals ANO10 mutations in patients with autosomal-recessive cerebellar ataxia. Am. J. Hum. Genet. *87*, 813–819.
28. Suzuki, J., Umeda, M., Sims, P.J., and Nagata, S. (2010). Calcium-dependent phospholipid scrambling by TMEM16F. Nature *468*, 834–838.
29. Caputo, A., Caci, E., Ferrera, L., Pedemonte, N., Barsanti, C., Sondo, E., Pfeffer, U., Ravazzolo, R., Zegarra-Moran, O., and Galietta, L.J. (2008). TMEM16A, a membrane protein associated with calcium-dependent chloride channel activity. Science *322*, 590–594.
30. Huang, W.C., Xiao, S., Huang, F., Harfe, B.D., Jan, Y.N., and Jan, L.Y. (2012). Calcium-activated chloride channels (CaCCs) regulate action potential and synaptic response in hippocampal neurons. Neuron *74*, 179–192.
31. Hartzell, C., Putzier, I., and Arreola, J. (2005). Calcium-activated chloride channels. Annu. Rev. Physiol. *67*, 719–758.
32. Cenedese, V., Betto, G., Celsi, F., Cherian, O.L., Pifferi, S., and Menini, A. (2012). The voltage dependence of the TMEM16B/anoctamin2 calcium-activated chloride channel is modified by mutations in the first putative intracellular loop. J. Gen. Physiol. *139*, 285–294.
33. Yang, Y.D., Cho, H., Koo, J.Y., Tak, M.H., Cho, Y., Shim, W.S., Park, S.P., Lee, J., Lee, B., Kim, B.M., et al. (2008). TMEM16A confers receptor-activated calcium-dependent chloride conductance. Nature *455*, 1210–1215.
34. Yu, K., Duran, C., Qu, Z., Cui, Y.Y., and Hartzell, H.C. (2012). Explaining calcium-dependent gating of anoctamin-1 chloride channels requires a revised topology. Circ. Res. *110*, 990–999.